Numerical Spectral Matrix Method for Propagation in General Layered Media: Application to Isotropic and Anisotropic Substrates

AYMAN A. MOSTAFA, STUDENT MEMBER, IEEE, CLIFFORD M. KROWNE, SENIOR MEMBER, IEEE, AND KAWTHAR A. ZAKI, SENIOR MEMBER, IEEE

Abstract—**A full-wave analysis technique for generalized anisotropic layered media based on a 4×4 field matrix method is applied to calculate the propagation constant of a number of microstriplike transmission structures. This technique is very versatile, and allows simultaneous permittivity, permeability, and optical activity anisotropy. Data for higher order modes of single and coupled strip lines in isotropic layered media in the millimeter-wave region are presented. New dispersion data for both low- and high-anisotropy dielectric layered structures are generated for different principal axis crystallographic orientations.**

I. Introduction

LAYERED STRUCTURES with general complex anisotropy cannot be handled by a transverse resonance approach (TRA) [1] or approaches which specialize anisotropy to particular cases such as magnetic birefringence. The transverse resonance approach, for example, is an acceptable method for isotropic layers or very simple anisotropic layers with carefully chosen principal axis orientation. A properly oriented uniaxial crystal could be analyzed by an extension of the TRA [2]. A much more powerful technique is available [3] which describes the fields by four-element field vectors and employs a 4×4 matrix in the spectral domain. This matrix method can allow simultaneous permittivity, permeability, and optical activity anisotropy. The displacement field vector can generally be described by both a permittivity tensor and an optical activity tensor. Likewise, the magnetic displacement vector can generally be described by a permeability tensor and an optical activity tensor. Each layer is characterized by a single constant 6×6 macroscopic tensor.

The ability to handle arbitrary materials with varying degrees of anisotropy is an important facet of the method. This capability includes accounting for principal axes crystallographic rotation on each layered material's constitutive tensors [4] by incorporating this information into each 6×6 macroscopic tensor. Although much analytic and numerical effort has been devoted previously in the literature to finding the behavior of uniaxial lossless dielectric guided-wave structures under quasi-static conditions, some work has been done in the area of fully dynamic dispersive studies [5]. Relatively recent studies of broadside-coupled strip lines [6] and single microstrip lines and bilateral finlines [7] using uniaxial substrates perform numerical dispersion studies with crystallographic permittivity principal axis rotation for the fundamental modes. No studies to our knowledge treat dispersion for the higher order modes under rotation. The fundamental modes as well as the higher order modes were found by tracing the mode curves from either the cutoff frequency or some point along the $\omega-\beta$ diagram. A contour integration procedure is used, whenever it is needed, to verify that a particular root is, in fact, a real solution or zero of the determinant.

In this paper we provide numerical results for single and coupled microstrip line on an isotropic substrate as well as on a low- and high-anisotropy dielectric material. The propagation constant γ for propagating waves ($\gamma = -j\beta$) is given for different principal axis crystallographic orientations θ of the permittivity tensor. This is done for the fundamental and higher order even and odd modes.

II. Analysis

Consider the multilayer structure shown in Fig. 1, in which each layer is characterized by a single 6×6 macroscopic tensor M representing the permittivity $\bar{\bar{\epsilon}}$, permeability $\bar{\bar{\mu}}$, and optical activity tensors $\bar{\bar{\rho}}$ and $\bar{\bar{\rho}}'$. An arbitrary number of perfectly conducting strips with zero thickness, equal width, and the same periodic spacing are assumed at the interfaces between two consecutive layers. Analysis of an open or a closed bilateral structure (having either perfect electrical walls [pew] or perfect magnetic walls [pmw]), is the same up to the final step of generating the elements of the final truncated matrix. The difference is that the integration for the open structure is carried out with respect to continuous spectral wave number α along

Manuscript received April, 9, 1987; revised July 16, 1987. This work was supported in part by NRL Contract N00014-86K-2013.

A. M. Mostafa and K. A. Zaki are with the Department of Electrical Engineering, University of Maryland, College Park, MD 20742.

C. M. Krowne is with the Electronics Technology Division, Naval Research Laboratory, Washington, DC 20375-5000.

IEEE Log Number 8717115.

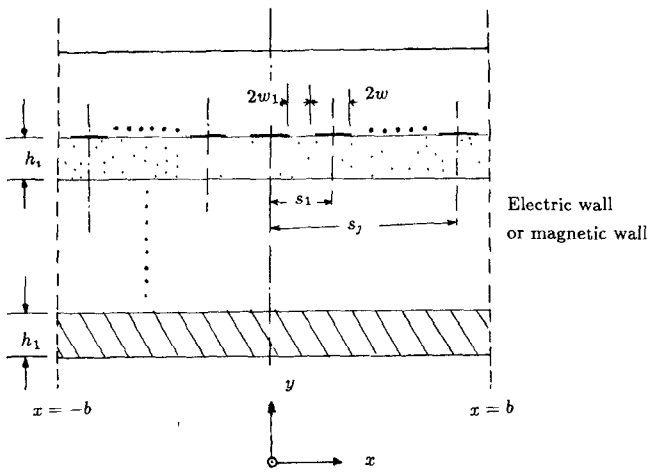

Fig. 1. Anisotropic layered media inside a shielded structure.

the x direction, while a summation for discrete spectral numbers is used for the finite enclosed structure. In the following analysis, pew's are assumed to be spaced b from the plane of symmetry to avoid the dimensional contour integration (and surface wave excitation), which is normally more difficult to perform than carrying out the summation.

A. Basic Equations

Assume that the propagation constant of the guided structure is γ and that the fields are time harmonic with dependence $e^{j\omega t}$. The Maxwell equations in the vector form are

$$\nabla \times \vec{E} = -j\omega\vec{B} \tag{1}$$

$$\nabla \times \vec{H} = j\omega\vec{D} \tag{2}$$

where the volume source currents within any layer are assumed to be zero. All the field components have the same propagation factor $e^{(j\omega t-\gamma z)}$ along the $+z$ direction of propagation, but for simplicity the time dependence will be dropped out through the analysis. The Fourier transform domain (FTD) fields are defined by taking the one-dimensional finite Fourier transform as

$$\tilde{f}(\alpha_n, y) = \int_{-b}^{b} f(x, y)e^{-j\alpha_n x}\,dx \tag{3}$$

where the tilde $\tilde{}$ denotes the Fourier transform, and α_n are discrete and equal to $(2n-1)\pi/2b$ or $n\pi/b$ for even or odd modes, respectively. Maxwell equations (1), (2) can be rewritten as [3]

$$\tilde{\Omega}\tilde{\phi}_L = j\omega\tilde{\phi}_R \tag{4}$$

where the $\tilde{\Omega}$ operator is expressed as

$$\tilde{\Omega} = \begin{bmatrix} 0 & \tilde{\Omega}_1 \\ -\tilde{\Omega}_1 & 0 \end{bmatrix} \qquad \tilde{\Omega}_1 = \begin{bmatrix} 0 & \gamma & \dfrac{d}{dy} \\ -\gamma & 0 & -j\alpha_n \\ -\dfrac{d}{dy} & j\alpha_n & 0 \end{bmatrix} \tag{5}$$

and the left and the right column vectors $\tilde{\phi}_L, \tilde{\phi}_R$ contain the electric and magnetic field components

$$\tilde{\phi}_L = \begin{bmatrix} \tilde{E}_x & \tilde{E}_y & \tilde{E}_z & \tilde{H}_x & \tilde{H}_y & \tilde{H}_z \end{bmatrix}^T$$

$$\tilde{\phi}_R = \begin{bmatrix} \tilde{D}_x & \tilde{D}_y & \tilde{D}_z & \tilde{B}_x & \tilde{B}_y & \tilde{B}_z \end{bmatrix}^T. \tag{6}$$

Each medium is characterized by a single 6×6 constitutive tensor M

$$\tilde{\phi}_R = M\tilde{\phi}_L \qquad M = \begin{bmatrix} \bar{\bar{\epsilon}} & \bar{\bar{\rho}} \\ \bar{\bar{\rho}}' & \bar{\bar{\mu}} \end{bmatrix}. \tag{7}$$

When (7) is substituted into (4), a linear system of coupled differential equations for the independent field components is obtained:

$$\tilde{\Omega}\tilde{\phi}_L = j\omega M\tilde{\phi}_L. \tag{8}$$

Two equations of the system (8) can be used to express $\tilde{E}_y$ and $\tilde{H}_y$ in terms of the other components of the vector $\tilde{\phi}_L$. This process leads to the matrix differential equation

$$\frac{d\tilde{\Phi}}{dy} = j\omega R\tilde{\Phi} \tag{9}$$

where the vector $\tilde{\Phi}$ is the four-element transformed field vector containing fields tangential to the interface

$$\tilde{\Phi} = \begin{bmatrix} \tilde{E}_x & \tilde{E}_z & \tilde{H}_x & \tilde{H}_z \end{bmatrix}^T \tag{10}$$

and R is a 4×4 matrix whose elements are function of ω, α_n, γ, and the medium properties M. Equation (9) is in the form of the state equations of a linear system [8], with the state vector $\tilde{\Phi}$ and the state matrix $A = j\omega R$. Equation (9) holds for the field components in each layer of the structure and has, in general, four distinct eigenvalues and four corresponding eigenvectors. The eigenvalues represent the propagation constants k_{yi}, $i=1,2,3,4$, while each eigenvector provides the ratio between the elements of the vector $\tilde{\Phi}$. This equation is general, and leads to special cases. For example, if $\bar{\bar{\epsilon}}$ is used for uniaxial material, the four coupled linear differential equations of (9) reduce to the fourth-order differential equation of [9] with the same eigenvalues.

In the ith layer, the solution of (9) can be expressed as

$$\tilde{\Phi}(y_i') = P(y_i')\tilde{\Phi}(0) \tag{11}$$

where $P(y_i')$ is the state transition matrix of the ith layer given by

$$P(y_i') = e^{Ay_i'} \tag{12}$$

and $\tilde{\Phi}(0)$ is the state vector at the interface $y_i' = 0$, i.e., at the bottom of the ith layer. The state transition matrix P is 4×4 and is recognized as a transformation operator which transforms the field from $y_i' = 0$ to the field value at y_i' within the ith layer.

The transformation operator $P(y)$ can be calculated by first finding the transverse eigenvalues k_{yi} of A and then applying the Cayley–Hamilton theorem [8] to the matrix A. As is shown in Appendix I, $P(y)$ can be expressed as

$$P(y) = \sum_{i=0}^{3} a_i A^i. \tag{13}$$

In general, the eigenvalues may be degenerate. The unknown coefficients a_i, which are functions of y, can be found by solving the system of linear equations

$$e^{k_{yj}y} = \sum_{i=0}^{3} a_i k_{yj}^i, \qquad j=1,2,3,4. \tag{14}$$

For the case of repeated (degenerate) eigenvalues, the derivatives of (14) are applied. For example, for the isotropic case we have two distinct eigenvalues of multiplicity $m=2$ each. Equation (14) turns out to be

$$\begin{bmatrix} 1 & k_{y1} & k_{y1}^2 & k_{y1}^3 \\ 0 & 1 & 2k_{y1} & 3k_{y1}^2 \\ 1 & k_{y2} & k_{y2}^2 & k_{y2}^3 \\ 0 & 1 & 2k_{y2} & 3k_{y2}^2 \end{bmatrix} \begin{bmatrix} a_0 \\ a_1 \\ a_2 \\ a_3 \end{bmatrix} = \begin{bmatrix} e^{k_{y1}y} \\ ye^{k_{y1}y} \\ e^{k_{y2}y} \\ ye^{k_{y2}y} \end{bmatrix}. \tag{15}$$

B. Boundary Conditions

Equation (11) relates the field components at any point within the ith layer to their value at the boundary of that region ($y_i' = 0$).

The boundary conditions applied at the interface $y = h_i$ in the Fourier transform domain are

$$\tilde{H}_x(h_i^+) - \tilde{H}_x(h_i^-) = -\tilde{J}_z \tag{16a}$$

$$\tilde{H}_z(h_i^+) - \tilde{H}_z(h_i) = \tilde{J}_x. \tag{16b}$$

$\tilde{J}_z$ and $\tilde{J}_x$ are the unknown Fourier-transformed x and z current components at $y = h_i$. The tangential electrical field components $\tilde{E}_z, \tilde{E}_x$ must be continuous along the interface. The + and − superscripts in (16) denote, respectively, just above and below the interface $y = h_i$. The boundary conditions could be expressed in the vector form

$$\tilde{\Phi}(h_i^+) = \tilde{\Phi}(h_i^-) + \begin{bmatrix} 0 \\ 0 \\ -\tilde{J}_z \\ \tilde{J}_x \end{bmatrix}. \tag{17}$$

C. Green's Functions and the Moment Method

The formulation for two dielectric media with current strips located at the interface will be derived here for demonstration. Generalization to multidielectric layers with several current strip interfaces is a straightforward procedure that follows the derivation here. The vector field $\tilde{\Phi}(h_1^-)$ can be related to $\tilde{\Phi}(0)$ through the transformation operator P of (11), i.e.,

$$\tilde{\Phi}(h_1^-) = P^{(1)}(h_1)\tilde{\Phi}(0). \tag{18}$$

The boundary conditions (17) at the interface $y = h_1$ could be written as

$$\tilde{\Phi}(h_1^+) = P^{(1)}(h_1)\tilde{\Phi}(0) + \begin{bmatrix} 0 \\ 0 \\ -\tilde{J}_z \\ \tilde{J}_x \end{bmatrix}. \tag{19}$$

Again, $P^{(2)}(h_2)$ transforms the field vector $\tilde{\Phi}(h_1^+)$ just above the interface $y = h_1$ to give the field vector at the top plane $y = h_1 + h_2$ such that

$$\tilde{\Phi}(h_1+h_2) = P^{(2)}(h_2)P^{(1)}(h_1)\tilde{\Phi}(0) + P^{(2)}(h_2)\begin{bmatrix} 0 \\ 0 \\ -\tilde{J}_z \\ \tilde{J}_x \end{bmatrix}. \tag{20}$$

Using the abbreviation $P^{(21)}(h_1 + h_2) = P^{(2)}(h_2)P^{(1)}(h_1)$, where $P^{(21)}$ is a 4×4 matrix, (20) could be rewritten as

$$\begin{bmatrix} 0 \\ 0 \\ \tilde{H}_x(h_1+h_2) \\ \tilde{H}_z(h_1+h_2) \end{bmatrix} = P^{(21)}(h_1+h_2)\begin{bmatrix} 0 \\ 0 \\ \tilde{H}_x(0) \\ \tilde{H}_z(0) \end{bmatrix} + P^{(2)}(h_2)\begin{bmatrix} 0 \\ 0 \\ -\tilde{J}_z \\ \tilde{J}_x \end{bmatrix}. \tag{21}$$

$\tilde{H}_x(0)$, $\tilde{H}_z(0)$, $\tilde{H}_x(h_1+h_2)$, and $\tilde{H}_z(h_1+h_2)$ are the tangential magnetic fields at the ground and top plate, respectively. Note that the boundary conditions at $y = h_2 + h_1$ have already been satisfied in (21). From (21) we can express $\tilde{H}_x(0)$, $\tilde{H}_z(0)$, in terms of $\tilde{J}_x$, $\tilde{J}_z$. Also from the first and second row of (19) we can express the slot field $\tilde{E}_x(h_1)$, $\tilde{E}_z(h_1)$ in terms of $\tilde{H}_x(0)$, $\tilde{H}_z(0)$, as in Appendix II. The resulting relationships define the impedance-type Green's function G in the FTD which relates the field components at the interface to the interface currents at $y = h_1$:

$$\tilde{E}_x(n) = \tilde{G}_{11}(\gamma, n)\tilde{J}_x(n) + \tilde{G}_{12}(\gamma, n)\tilde{J}_z(n) \tag{22a}$$

$$\tilde{E}_z(n) = \tilde{G}_{21}(\gamma, n)\tilde{J}_x(n) + \tilde{G}_{22}(\gamma, n)\tilde{J}_z(n) \tag{22b}$$

where the elements $\tilde{G}_{ij}$ are given in Appendix II. For the three-layer structure shown in Fig. 4, the above procedure is still applied, with some relevant replacements given also in Appendix II.

Expanding the strip currents in (22) in terms of suitable basis functions and using a Galerkin-like approach, a determinantal equation for the propagation constant can be written based on the fact that the current expansion coefficients are not a trivial null set. For example, for n_s strips the following expansions were employed for even modes (see derivation in Appendix III):

$$\tilde{J}_z(n) = \sum_{j=1}^{n_{ss}} \sum_{i=1}^{n_z} \left[a_{ij}\cos(\alpha_n s_j)\tilde{\xi}_{ei}(n) + b_{ij}\sin(\alpha_n s_j)\tilde{\xi}_{oi}(n) \right] \tag{23a}$$

$$\tilde{J}_x(n) = \sum_{j=1}^{n_{ss}} \sum_{i=1}^{n_x} \left[c_{ij}\cos(\alpha_n s_j)\tilde{\eta}_{oi}(n) + d_{ij}\sin(\alpha_n s_j)\tilde{\eta}_{ei}(n) \right]. \tag{23b}$$

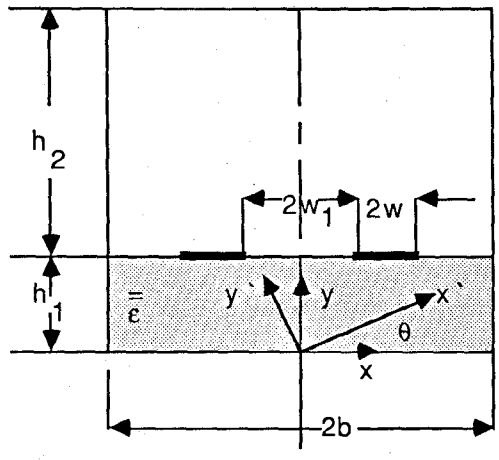

Fig. 2. Coupled microstrip lines.

For odd modes, the expansions were

$$\tilde{J}_z(n) = \sum_{j=1}^{n_{ss}} \sum_{i=1}^{n_z} \left[a_{ij} \sin(\alpha_n s_j) \tilde{\xi}_{ei}(n) + b_{ij} \cos(\alpha_n s_j) \tilde{\xi}_{oi}(n) \right] \quad (24a)$$

$$\tilde{J}_x(n) = \sum_{j=1}^{n_{ss}} \sum_{i=1}^{n_x} \left[c_{ij} \cos(\alpha_n s_j) \tilde{\eta}_{ei}(n) + d_{ij} \sin(\alpha_n s_j) \tilde{\eta}_{oi}(n) \right] \quad (24b)$$

where $n_{ss} = n_s/2$, $(n_s - 1)/2$ for even and odd number of strips n_s respectively, and n_z, n_x are the number of basis functions for $\tilde{J}_z$ and $\tilde{J}_x$. Here the spacing factor s_j is the distance from the origin to the center of the jth strip and $\alpha_n = (2n-1)\pi/2b, n\pi/b$ for even and odd modes, respectively. The quantities $\tilde{\xi}_e, \tilde{\xi}_o, \tilde{\eta}_e, \tilde{\eta}_o$ are single microstrip even and odd basis functions of $\tilde{J}_z$ and $\tilde{J}_x$, respectively [10].

D. Rotation around the Principal Axis

To investigate the effect of misalignment, rotations of the principal axes are performed [4]. Propagation properties in the rotated system are easily obtained using the above-described method, provided the proper transformed constitutive tensor M is used. Consider the principal axis rotation shown in Fig. 2, where a rotation is made around the z axis through an angle θ, i.e., in the transverse plane. Let us assume that $0x', 0y', 0z$ are the principal axes with

$$\bar{\bar{\epsilon}}' = \begin{bmatrix} \epsilon_1 & 0 & 0 \\ 0 & \epsilon_2 & 0 \\ 0 & 0 & \epsilon_3 \end{bmatrix}. \quad (25)$$

In the xyz system we have

$$\bar{\bar{\epsilon}} = \begin{bmatrix} \epsilon_{xx} & \epsilon_{xy} & 0 \\ \epsilon_{yx} & \epsilon_{yy} & 0 \\ 0 & 0 & \epsilon_{zz} \end{bmatrix} \quad (26)$$

where

$$\begin{aligned} \epsilon_{xx} &= \epsilon_2 \sin^2(\theta) + \epsilon_1 \cos^2(\theta) \\ \epsilon_{yy} &= \epsilon_2 \cos^2(\theta) + \epsilon_1 \sin^2(\theta) \\ \epsilon_{zz} &= \epsilon_3 \\ \epsilon_{xy} &= \epsilon_{yx} = (\epsilon_2 - \epsilon_1) \sin\theta \cos\theta. \end{aligned} \quad (27)$$

The effect of varying the rotation angle θ can thus be obtained systematically when the above transformation tensor is used in the previous formulation.

III. Numerical Results

In the numerical search for the zeros of the determinantal equation, it is often necessary to determine whether a certain contour contains any zeros, and if so, how many. Such a determination can be done using a contour integration procedure. This method makes use of the principle of argument formula:

$$\oint_c \frac{D'(\beta)}{D(\beta)} d\beta = j2\pi(N - P). \quad (28)$$

N and P are the number of zeros and poles of the determinant D inside the contour c, respectively. Here $D(\beta)$ is an analytic function within the contour except at its poles. This contour integration method is very powerful and useful in determining the location of the zeros and their degree (degenerate modes) if the locations of the poles are given.

Convergence behavior has been tested and is demonstrated in Fig. 3 (the parameters employed being $\epsilon_1 = \epsilon_3 = 9.4$, $\epsilon_2 = 11.6$, substrate thickness $h_1 = 0.5$ mm and $h_2 = 4.5$ mm, with $w/h_1 = 0.5$) by showing the variation of $\bar{\beta} = \beta/k_0$ (k_0 = free-space wavenumber) versus spectral number n. It is seen that 70 spectral terms are reasonable for accurate solution and fast computation. Tables I and II give $\bar{\beta}$ at three frequencies for varying basis function number on each strip and show that agreement between the $\bar{\beta}$ values is at the fourth digit, leading us to use only the $n_x, n_z = (1,1)$ for efficient computation.

Numerical $\bar{\beta}$ results are presented in Fig. 4 for suspended coupled microstrip over an isotropic substrate. The solution for even higher order modes on a single microstrip line with the same parameters given in reference [11] agrees closely with the results in [11]. Because alumina, silicon, GaAs, and many other common materials used in hybrid and monolithic circuits have dielectric constants ϵ_r on the order of 10, we study the particular case $\epsilon_r = 9.35$ and the dimensions found in the literature [12]. Results for the higher order modes, of interest in millimeter-wave applications, up to 35 GHz are presented in Fig. 4(a) and (b) for even and odd modes of suspended coupled microstrip, respectively. These results were also checked with the method described in [1] and agreement was within a few percent. The parameters used for Fig. 4 are $h_1 = h_3 = 4.5$ mm, $h_2 = 1.0$ mm, $w = w_1 = 1.0$ mm, $2b = 20$ mm, $\epsilon_r = 9.35$, and $\epsilon_{r1} = \epsilon_{r3} = 1.0$. For the dominant even and odd modes, agreement between our method and reference [12] is within a few percent.

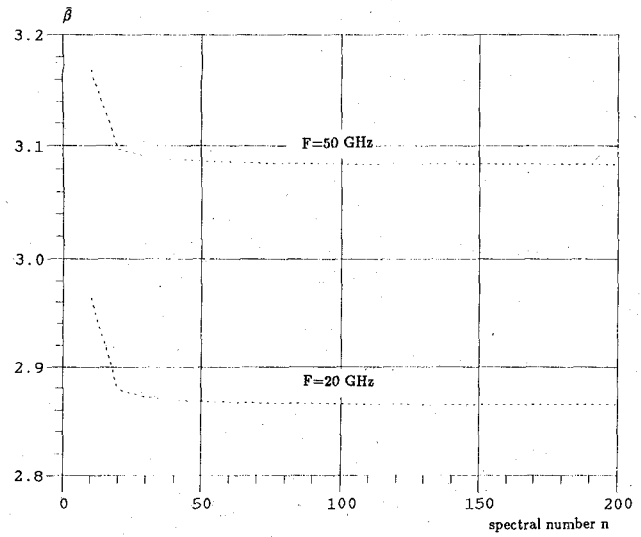

Fig. 3. $\bar{\beta}$ versus spectral number n. $h_1 = 0.5$ mm, $h_2 = 4.5$ mm with $w/h_1 = 0.5$ for the fundamental even mode [15].

TABLE I
ODD MODES FOR THE PARAMETERS USED IN FIG. 5

$\bar{\beta}$ for different (n_x, n_z)				
F(GHz)	(1,1)	(1,2)	(2,1)	(2,2)
2	2.5177	2.5176	2.5179	2.5176
10	2.6946	2.6947	2.6947	2.6946
20	2.9927	2.9921	2.9928	2.9921

TABLE II
EVEN MODES FOR THE PARAMETERS USED IN FIG. 5

$\bar{\beta}$ for different (n_x, n_z)				
F(GHz)	(1,1)	(1,2)	(2,1)	(2,2)
2	2.6884	2.6883	2.6886	2.6882
10	3.0412	3.0408	3.0412	3.0406
20	3.2046	3.2031	3.2047	3.2031

Data have been generated for single and coupled microstrip line structures which employ anisotropic sapphire substrates. Since sapphire has only a moderate degree of anisotropy (about 21 percent), data are also gathered on an interesting substrate material which has much higher anisotropy (about 40.4 percent), pyrolytic boron nitride (PBN). This material originally stimulated interest because it had reasonable characteristic line impedance [13] for integrated circuit applications and might enable even- and odd-mode phase velocity differences to be reduced in coupled line structures [13], [14]. Single and coupled line structures using PBN were studied in terms of material properties, predicted electrical behavior, and measured performance [14], and may be useful for hybrid integrated circuits.

For single microstrip lines over sapphire, agreement between our results and [15] having a bilateral open structure for the cases where $2w/h = 1$, 2, and 4 is within 0.5 percent when the side wall width ($2b$) is ten times the substrate thickness (h_1). For coupled microstrip over sapphire, the even and odd fundamental mode dispersion results agree within 1 percent with [2]. PBN dispersion

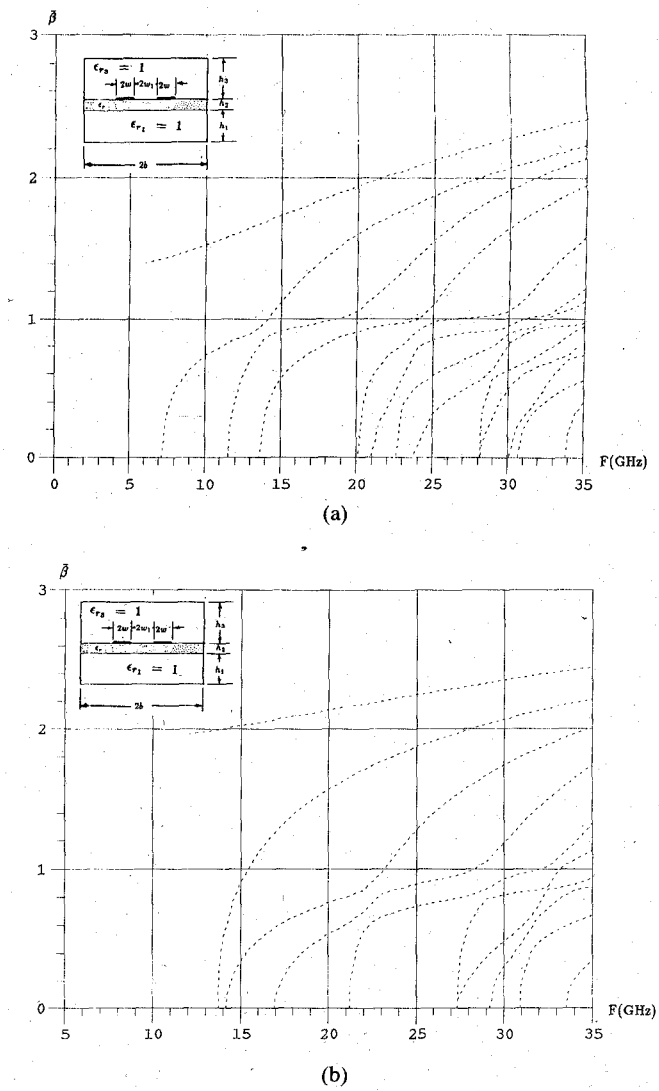

Fig. 4. (a) Dispersion curves ($\bar{\beta}-F$) for even modes. $h_1 = h_3 = 4.5$ mm, $h_2 = 1$ mm, $w = w_1 = 1$ mm, $\epsilon_r = 9.35$. (b) Dispersion curves ($\bar{\beta}-F$) for odd modes. $h_1 = h_3 = 4.5$ mm, $h_2 = 1$ mm, $w = w_1 = 1$ mm, $\epsilon_r = 9.35$.

curves for coupled microstrip for even and odd modes up to 20 GHz are shown in Fig. 5. The parameters used were $\epsilon_1 = \epsilon_3 = 5.12$, $\epsilon_2 = 3.40$, $2w = 1.5$ mm, $2w_1 = 1.5$ mm, substrate thickness $h_1 = 1.5$ mm, $h_2 = 3$ mm, and $2b = 8.5$ mm. Notice that the first higher order mode is even.

Numerical results have been checked by varying θ against the quasi-static data available in the literature [16], with good agreement, as shown in Fig. 6. The parameters used were $\epsilon_1 = \epsilon_3 = 40$, $\epsilon_2 = 10$, $w = w_1 = 0.5\, h_1$, $h_2/h_1 = 2$, and frequency $F = 1$ GHz. For the same configuration as in Fig. 2, $\bar{\beta}$ versus frequency is plotted in Fig. 7 as a function of θ, for the fundamental mode at $F = 10$ and 20 GHz. The parameters used were the same as those in Fig. 5. Dispersion curves showing $\bar{\beta}$ versus frequency up to 40 GHz for $\theta = 0°$, 45°, and 90° are given in Figs. 8–10, respectively, with the same parameters as in Fig. 5. The following principal axes (diagonal) relative permittivity tensor elements were used [14]: $\epsilon_1 = \epsilon_3 = 5.12$, $\epsilon_2 = 3.14$. For the even fundamental mode, $\bar{\beta}$ shifts by a maximum of 20 percent relative to $\bar{\beta}$ at $\theta = 0$. Cutoff frequency f_c for

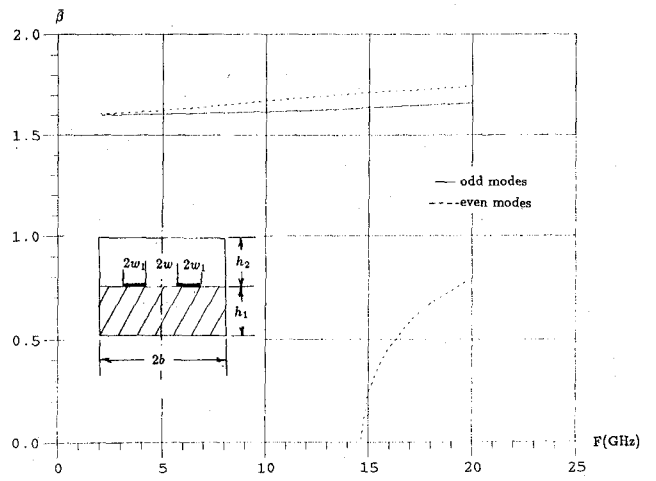

Fig. 5. Dispersion curves ($\bar{\beta}-F$) for coupled strip lines over PBN substrate. $h_1 = 1.5$ mm, $h_2 = 3$ mm, $2b = 8.5$ mm, $w = w_1 = 0.75$ mm.

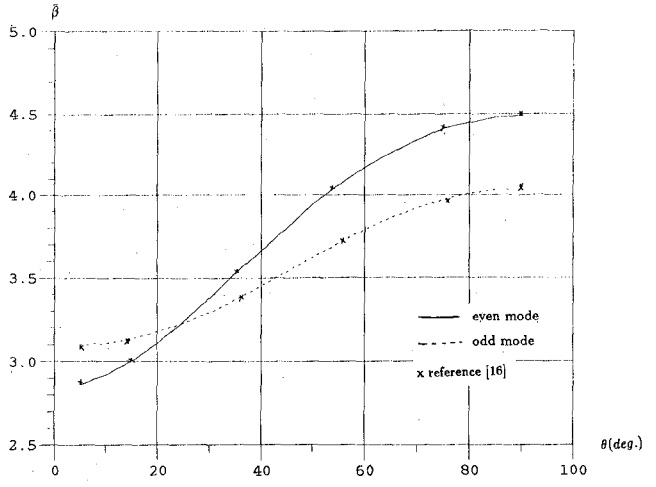

Fig. 6. Dispersion curves ($\bar{\beta}-\theta$) for coupled strip lines for the fundamental modes. $\epsilon_1 = \epsilon_3 = 40$, $\epsilon_2 = 10$, $w = w_1 = 0.5h_1$, $h_2/h_1 = 2$, and $F = 1$ GHz.

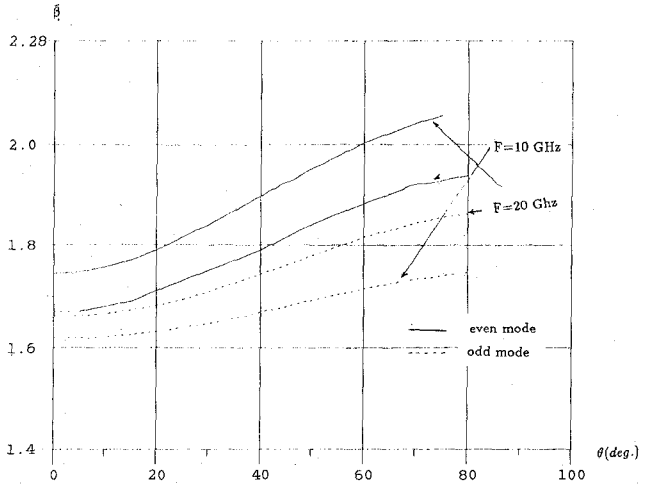

Fig. 7. Dispersion curves ($\bar{\beta}-\theta$) for the fundamental modes. $h_1 = 1.5$ mm, $h_2 = 3$ mm, $w = w_1 = 0.75$ mm, and $2b = 8.5$ mm.

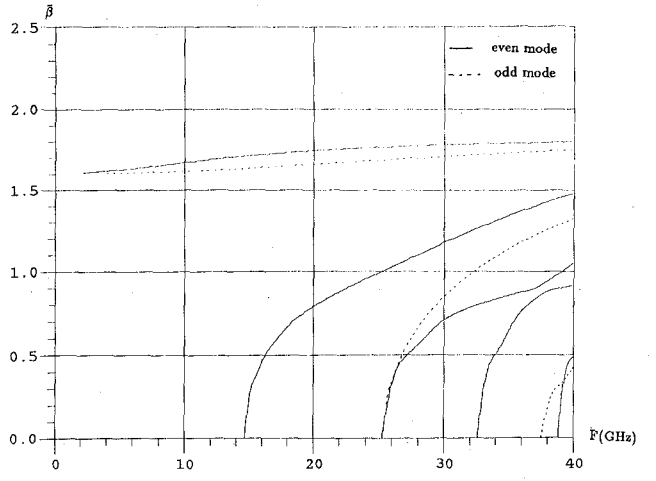

Fig. 8. Dispersion curves ($\bar{\beta}-F$) for even and odd modes for $\theta = 0°$. Same parameters as in Fig. 7.

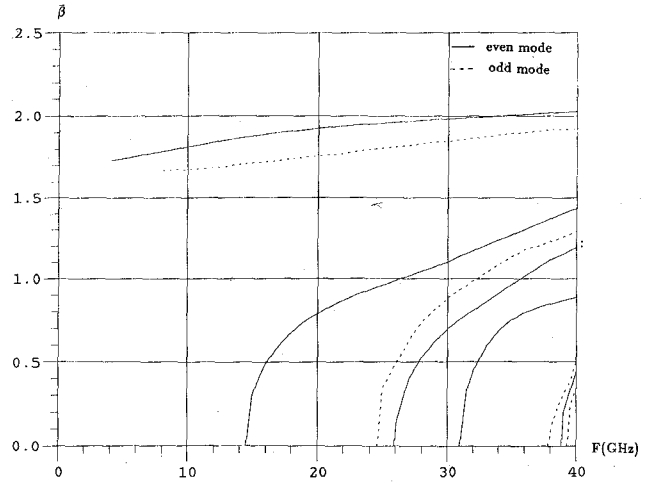

Fig. 9. Dispersion curves ($\bar{\beta}-F$) for even and odd modes for $\theta = 45°$. Same parameters as in Fig. 7.

the higher even order modes is insensitive to θ variation, except for the third higher order mode (fourth mode), which changes by 2 GHz when θ changes from 0° to 90°. The effect of changing θ from 0° to 90° is to increase the coupling between the 2nd and the 3rd modes, and to decrease the coupling between the 3rd and 4th modes. No significant fundamental-to-1st mode coupling is observed due to either frequency or θ variation. However, at frequencies higher than 40 GHz this coupling may be appreciable. For the odd modes, $\bar{\beta}$ shifts by a maximum of 18%, for the fundamental mode, relative to $\bar{\beta}$ at $\theta = 0$. For $\theta = 45°$ and 90° a new 4th mode appears. This mode shows increasingly coupling to the 3rd mode as θ increases beyond 45°.

Behavior of $\bar{\beta}$ on geometrical parameters is shown in Figs. 11–13 for specific θ cases for the fundamental mode. Fig. 11 gives the dependence of $\bar{\beta}$ on the height of the top plate h_2/h_1. Beyond $h_2/h_1 = 2$, $\bar{\beta}$ varies little. Fig. 12 displays the $\bar{\beta}$ dependence on the strip width $2w/h_1$. A similar plot is given in Fig. 13 showing $\bar{\beta}$ versus the strip spacing $2w_1/h_1$.

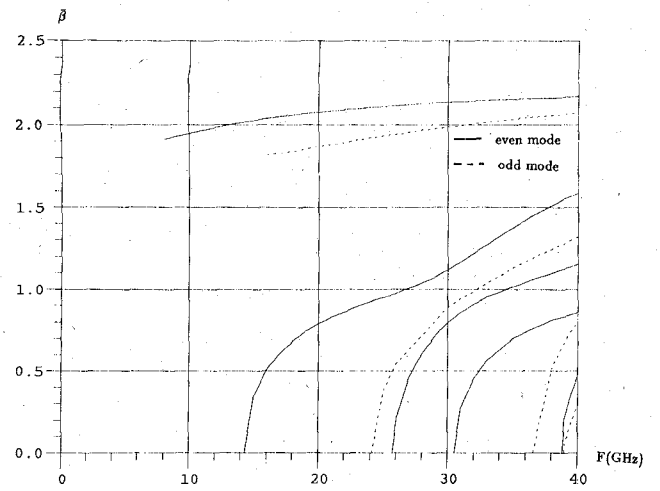

Fig. 10. Dispersion curves ($\bar{\beta}-F$) for even and odd modes for $\theta = 90°$. Same parameters as in Fig. 7.

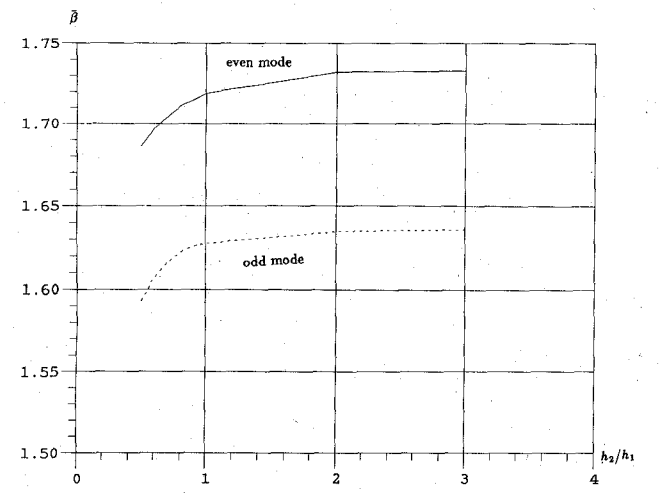

Fig. 11. Variation of $\bar{\beta}$ with h_2/h_1 for $\theta = 0°$ for coupled microstrip lines over PBN substrate for the fundamental modes. $w = w_1 = 0.25h_1$, $h_1 = 1.5$ mm, $F = 20$ GHz.

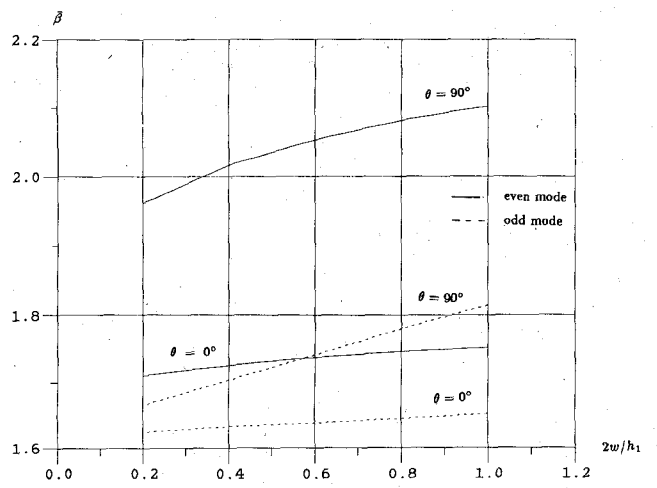

Fig. 12. Variation of $\bar{\beta}$ with $2w/h_1$ for $\theta = 0°$, 90° for coupled microstrip lines over PBN substrate for the fundamental modes. $2w_1/h_1 = 0.5$, $h_1 = 1.5$ mm, $2b = 8.5$ mm, $F = 20$ GHz, and $h_2 = 3$ mm.

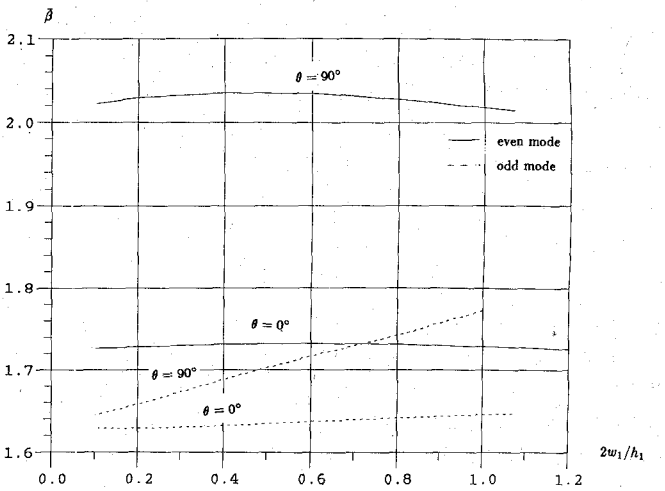

Fig. 13. Variation of $\bar{\beta}$ with $2w_1/h_1$ for $\theta = 0°$, 90° for coupled microstrip lines over PBN substrate for the fundamental modes. $2w/h_1 = 0.5$, $h_1 = 1.5$ mm, $2b = 8.5$ mm, $F = 20$ GHz, and $h_2 = 3$ mm.

IV. Conclusions

Numerical implementation of a general 4×4 matrix technique to find the propagation characteristics of strips immersed in either isotropic or anisotropic media has been demonstrated. The accuracy of the implementation has been checked and found to agree with the previous calculations for some special cases. Numerical results for a highly anisotropic layered structure are presented. The effect of changing rotation angle θ on the dispersion behavior of the fundamental and higher order even and odd modes was provided. Although data presented in this paper dealt only with the propagation characteristics in generalized anisotropic multilayered media, characteristic impedance computation is also possible using the same formulation. This can be done by calculating the currents on the conductors and the power flow in the structure.

Appendix I

The characteristic polynomial of an $n\times n$ matrix is defined as

$$\Delta(\lambda) = |A - \lambda I| = (-\lambda)^n + C_{n-1}\lambda^{n-1} + \cdots + C_1\lambda + C_0 = 0. \quad \text{(A1)}$$

This equation is satisfied by the eigenvalue λ_i. Now if $P(\lambda)$ is a scalar polynomial of degree m and $P_1(\lambda)$ is another polynomial of degree n where $n < m$, then $P(\lambda)$ can be written as

$$P(\lambda) = Q(\lambda)P_1(\lambda) + R(\lambda). \quad \text{(A2)}$$

The quotient $Q(\lambda)$ is a polynomial of degree of $m-n$ and the remainder polynomial $R(\lambda)$ is of degree of $n-1$. If we choose $P(\lambda)$ to be any analytic function and $P_1(\lambda)$ to be the characteristic polynomial, then

$$P(\lambda_i) = R(\lambda_i). \quad \text{(A3)}$$

This is the Cayley-Hamilton theorem, which states that every matrix satisfies its own characteristic equation, that is,

$$\Delta(A) = [0]. \quad \text{(A4)}$$

Making use of the above theorem (A4) and using a matrix function argument in (A3), one can express any analytic function of a matrix $P(A)$ as

$$P(A) = a_0 I + a_1 A + a_2 A^2 + \cdots + a_{n-1} A^{n-1}. \quad \text{(A5)}$$

The coefficients a_i are the same for the corresponding eigenfunction equation

$$P(\lambda_i) = R(\lambda_i) = a_0 + a_1 \lambda_i + a_2 \lambda_i^2 + \cdots + a_{n-1} \lambda_i^{n-1}. \quad \text{(A6)}$$

If the n eigenvalues are distinct, we get n independent algebraic equations that determine the coefficients a_i. However if we have repeated eigenvalues λ_i of a multiplicity order of m_i, then we have $d^j/d\lambda^j \Delta(\lambda)|_{\lambda_i} = 0$, where $j < m$; therefore

$$\left.\frac{d^j R(\lambda)}{d\lambda^j}\right|_{\lambda_i} = \left.\frac{d^j P(\lambda)}{d\lambda^j}\right|_{\lambda_i}, \qquad j = 1, \cdots, m_i - 1. \quad \text{(A7)}$$

We obtain a m_i set of linearly independent equations for λ_i from (A7); and thus a full set of n equations is always available to find a_i. If we choose $P(A) = e^{Ay}$, where A is 4×4, with repeated eigenvalues λ_1 of multiplicity $m_1 = 2$, then (A6) becomes

$$\begin{bmatrix} 1 & \lambda_1 & \lambda_1^2 & \lambda_1^3 \\ 0 & 1 & 2\lambda_1 & 3\lambda_1^3 \\ 1 & \lambda_2 & \lambda_2^2 & \lambda_2^3 \\ 1 & \lambda_3 & \lambda_3^2 & \lambda_3^3 \end{bmatrix} \begin{bmatrix} a_0 \\ a_1 \\ a_2 \\ a_3 \end{bmatrix} = \begin{bmatrix} e^{\lambda_1 y} \\ y e^{\lambda_1 y} \\ e^{\lambda_2 y} \\ e^{\lambda_3 y} \end{bmatrix}. \quad \text{(A8)}$$

Appendix II

From (21) we have

$$\tilde{H}_x(0) = \left[\tilde{J}_x\left(P_{24}^{(21)} P_{14}^{(2)} - P_{14}^{(21)} P_{24}^{(2)}\right) - \tilde{J}_z\left(P_{24}^{(21)} P_{13}^{(2)} - P_{14}^{(21)} P_{23}^{(2)}\right)\right]/\det \quad \text{(A9)}$$

$$\tilde{H}_z(0) = \left[\tilde{J}_x\left(P_{13}^{(21)} P_{24}^{(2)} - P_{23}^{(21)} P_{14}^{(2)}\right) - \tilde{J}_z\left(P_{13}^{(21)} P_{23}^{(2)} - P_{23}^{(21)} P_{13}^{(2)}\right)\right]/\det \quad \text{(A10)}$$

where $\det = P_{14}^{(21)} P_{23}^{(21)} - P_{13}^{(21)} P_{24}^{(21)}$. Also from (19)

$$\tilde{E}_x(h_1) = P_{13}^{(1)} \tilde{H}_x(0) + P_{14}^{(1)} \tilde{H}_z(0) \quad \text{(A11)}$$

$$\tilde{E}_z(h_1) = P_{23}^{(1)} \tilde{H}_x(0) + P_{24}^{(1)} \tilde{H}_z(0). \quad \text{(A12)}$$

Combining (A9), (A10), (A11), and (A12), we end up with the Fourier-transformed Green's function G:

$$\begin{aligned}
\tilde{G}_{11} &= \left[P_{13}^{(1)}\left(P_{24}^{(21)} P_{14}^{(2)} - P_{14}^{(21)} P_{24}^{(2)}\right) + P_{14}^{(1)}\left(P_{13}^{(21)} P_{24}^{(2)} - P_{23}^{(21)} P_{14}^{(2)}\right)\right]/\det \\
\tilde{G}_{12} &= -\left[P_{13}^{(1)}\left(P_{24}^{(21)} P_{13}^{(2)} - P_{14}^{(21)} P_{23}^{(2)}\right) + P_{14}^{(1)}\left(P_{13}^{(21)} P_{23}^{(2)} - P_{23}^{(21)} P_{13}^{(2)}\right)\right]/\det \\
\tilde{G}_{21} &= \left[P_{23}^{(1)}\left(P_{24}^{(21)} P_{14}^{(2)} - P_{14}^{(21)} P_{24}^{(2)}\right) + P_{24}^{(1)}\left(P_{13}^{(21)} P_{24}^{(2)} - P_{23}^{(21)} P_{14}^{(2)}\right)\right]/\det \\
\tilde{G}_{22} &= -\left[P_{23}^{(1)}\left(P_{24}^{(21)} P_{13}^{(2)} - P_{14}^{(21)} P_{23}^{(2)}\right) + P_{24}^{(1)}\left(P_{13}^{(21)} P_{23}^{(2)} - P_{23}^{(21)} P_{13}^{(2)}\right)\right]/\det
\end{aligned} \quad \text{(A13)}$$

where $P_{ij}^{(m)}$ denotes the ij element of m matrix, $m = 1$, 2, or 21 defined in the text.

For the three-layer structure, $P^{(1)}(h_1)$ is replaced by $P^{(21)} = P^{(2)}(h_2) P^{(1)}(h_1)$ and $P^{(2)}(h_2)$ is replaced by $P^{(3)}(h_3)$. Also $P^{(21)}(h_1 + h_2)$ is replaced by $P^{(31)} = P^{(3)}(h_3) P^{(2)}(h_2) P^{(1)}(h_1)$. Making use of these replacements and substituting into (A13) leads to the Green's function for the three-layer structure.

Appendix III

The currents J_z, J_x over any number of strips can be written as

$$J_z(x) = \sum_{j=1}^{n_{ss}} \left\{a_j \xi_{e_j}(x) + b_j \xi_{o_j}(x)\right\} + \sum_{j=1}^{n_{ss}} \left\{c_j \xi_{e_j}(x) + d_j \xi_{o_j}(x)\right\} \quad \text{(A14)}$$

$$J_x(x) = \sum_{j=1}^{n_{ss}} \left\{e_j \eta_{o_j}(x) + f_j \eta_{e_j}(x)\right\} + \sum_{j=1}^{n_{ss}} \left\{g_j \eta_{o_j}(x) + h_j \eta_{e_j}(x)\right\}. \quad \text{(A15)}$$

The quantity n_{ss} is already defined in the text. The first sum term in (A14) and (A15) accounts for those strips with $x > 0$, while the second sum term accounts for the strips with $x < 0$. The quantities $\xi_{e_j}, \xi_{o_j}, \eta_{e_j}, \eta_{o_j}$ are even and odd z and x basis current functions over the jth strip, respectively. The following discussion applies to the even-mode case. We have

$$J_z(x) = J_z(-x) \qquad J_x(x) = -J_x(-x) \quad \text{(A16)}$$

which results in

$$a_j = c_j \qquad b_j = d_j \qquad e_j = g_j \qquad \text{and} \qquad f_j = -h_j. \quad \text{(A17)}$$

The basis function $\xi_{e_j}(x)$, for example, can be expressed as

$$\xi_{e_j}(x) = \xi_e(x - s_j) \quad \text{(A18)}$$

where s_j is the spacing between the plane of symmetry and the center of the jth layer. By expressing the other basis functions in the same form, J_z, J_x could be rewritten from (A14) and (A15) as

$$J_z = \sum_{j=1}^{n_{ss}} a_j\left[\xi_e(x - s_j) + \xi_e(x + s_j)\right] + b_j\left[\xi_o(x - s_j) - \xi_o(x + s_j)\right] \quad \text{(A19)}$$

$$J_x = \sum_{j=1}^{n_{ss}} e_j\left[\eta_o(x - s_j) + \eta_o(x + s_j)\right] + f_j\left[\eta_e(x - s_j) - \eta_e(x + s_j)\right]. \quad \text{(A20)}$$

If the Fourier transforms are taken for both sides of (A19) and (A20), the currents J_x and J_z can be expressed in the Fourier transform domain. It is easy to show that

$$\tilde{\xi}_e(x \pm s_j) = e^{\pm j\alpha_n s_j} \tilde{\xi}_e. \quad \text{(A21)}$$

Identical transformation forms occur for the other basis functions. Applying the Fourier transform to (A19) and (A20) and making use of the Fourier shifting relationship (A21), one gets

$$\tilde{J}_z(n) = \sum_{j=1}^{n_{ss}} a_j \cos(\alpha_n s_j)\tilde{\xi}_e(n) + b_j \sin(\alpha_n s_j)\tilde{\xi}_o(n) \quad \text{(A22)}$$

$$\tilde{J}_x(n) = \sum_{j=1}^{n_{ss}} c_j \cos(\alpha_n s_j)\tilde{\eta}_o(n) + d_j \sin(\alpha_n s_j)\tilde{\eta}_e(n). \quad \text{(A23)}$$

Equations (A22) and (A23) are considered for only one basis function for J_z, J_x over each strip. A summation has to be added if more than one basis function is considered, as in (23) and (24) in the text.

The same procedure as above should be applied to the odd-mode case.

References

[1] T. Itoh, "Spectral-domain immittance approach for dispersion characteristics of generalized printed transmission lines," *IEEE Trans. Microwave Theory Tech.*, vol. MTT-28, pp. 733–736, July 1980.

[2] T. Kitazawa and Y. Hayashi, "Coupled slots on anisotropic sapphire substrates," *IEEE Trans. Microwave Theory Tech.*, vol. MTT-29, pp. 1035–1040, Oct. 1981.

[3] C. M. Krowne, "Fourier transformed matrix method of finding propagation characteristics of complex anisotropic layered media," *IEEE Trans. Microwave Theory Tech.*, vol. MTT-32, pp. 1617–1625, Dec. 1984.

[4] J. F. Nye, *Physical Properties of Crystals*. Oxford: Oxford University Press, 1979.

[5] N. G. Alexopoulos, "Integrated-circuit structures on anisotropic substrates," *IEEE Trans. Microwave Theory Tech.*, vol. MTT-33, pp. 847–881, Oct. 1985.

[6] T. Kitazawa, Y. Hayashi, K. Fujita, H. Mukaihara, "Analysis of broadside-coupled strip lines with anisotropic substrate," *Electronics Commun.*, vol. 66-B, pp. 82–90, 1983.

[7] R. Marques and M. Horno, "Dyadic Green's function for microstrip-like transmission lines on a large class of anisotropic substrates," *Proc. Inst. Elec. Eng.*, vol. 133, pt. H, pp. 450–454, Dec. 1986.

[8] N. Balabanian and T. A. Bickart, *Electrical Network Theory*. New York: Wiley, 1969; also T. E. Fortmann and K. L. Hitz, *An Introduction to Linear Control Systems*. New York: Marcel Dekker, 1977.

[9] C. M. Krowne, "Green's function in the spectral domain for biaxial and uniaxial anisotropic planar dielectric structures," *IEEE Trans. Antennas Propagat.*, vol. AP-32, pp. 1273–1281, Dec. 1984.

[10] C. M. Krowne, "Slow wave propagation in generalized cylindrical waveguides loaded with a semiconductor," *Int. J. Electron.*, vol. 58, pp. 249–269, Feb. 1985.

[11] E. E. Hassan, "Field solution, polarization, and eigenmodes of shielded microstrip transmission line," *IEEE Trans. Microwave Theory Tech.*, vol. MTT-34, pp. 845–852, Aug. 1986.

[12] E. Yamashita and K. Atsuki, "Analysis of microstrip-like transmission lines by nonuniform discretization of integral equations," *IEEE Trans. Microwave Theory Tech.*, vol. MTT-24, pp. 195–200, Apr. 1976.

[13] C. M. Krowne, "Microstrip transmission lines on pyrolytic boron nitride," *Electron. Lett.*, vol. 12, pp. 642–643, Nov. 1976.

[14] C. M. Krowne and T. E. Washburn, "Pyrolytic boron nitride as a microstrip substrate material," *IEEE Trans. Electrical Insulation*, vol. EI-14, pp. 111–116, Apr. 1979.

[15] A.-M. A. El-Sherbiny, "Hybrid mode analysis of microstrip lines on anisotropic substrates," *IEEE Trans. Microwave Theory Tech.*, vol. MTT-29, pp. 1261–1265, Dec. 1981.

[16] M. Horno, "Quasistatic characteristics of covered coupled microstrips on anisotropic substrate: Spectral and variational analysis," *IEEE Trans. Microwave Theory Tech.* vol. 30, pp. 1888–1892, Nov. 1982.

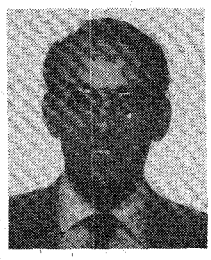

Ayman A. Mostafa (S'85) was born in Cairo, Egypt in 1959. He received the B.Sc. (with honors) and M.Sc degrees in electrical engineering from Ain Shams University, Cairo, in 1981 and 1984, respectively.

From 1981 to 1984 he was a Teaching Assistant in the Department of Electronics and Computer Engineering at Ain Shams University. From February 1985 to September 1985 he was a Research Associate at Duisburg University, West Germany. In September 1985 he joined the Electrical Engineering Department of the University of Maryland as a graduate Research Assistant and since then has been working towards the Ph.D degree. His research interests include the CAD of millimeter-wave circuits and numerical solutions of planar microwave structures.

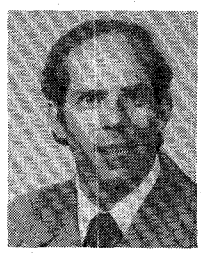

Clifford M. Krowne (S'73–M'74–SM'84) attended the University of California, Berkeley, and received the B.S. degree in physics from the University of California, Davis, in 1970 and the M.S. and Ph.D degrees in electrical engineering from the University of California, Los Angeles, in 1972 and 1975, respectively.

In 1970, he was employed in the Microelectronics Division of Lockheed Missiles and Space Company. In 1976 he joined the technical staff of the Watkins-Johnson Company in Palo Alto, CA, and in 1978 he became a faculty member of the Department of Electrical Engineering at North Carolina State University, Raleigh. Dr. Krowne has been a consultant to several industrial firms and was a 1980 ASEE Summer Faculty Fellow at the NASA Johnson Space Center, Houston, TX. Since 1981, he has been with the Electronics Technology Division of the Naval Research Laboratory, Washington, DC, studying microwave and millimeter-wave properties of active and passive solid-state devices. He is also an Adjunct Professor of Electrical Engineering, University of Maryland, College Park, MD.

Dr. Krowne has published over 80 technical papers in solid-state electronics, microwave circuits, electromagnetics, and engineering education. He has served on the technical program conference committees of the Antennas and Propagation Society and the Microwave Theory and Techniques Society and chaired sessions in the electromagnetic theory, microstrip antenna, and solid-state devices/circuits areas. Dr. Krowne was a member of the 1987 MTT Symposium steering committee. He is a member of Phi Kappa Phi, Tau Beta Pi, and the American Physical Society.

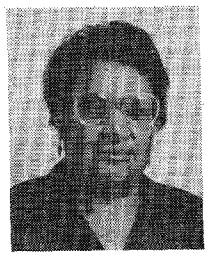

Kawthar A. Zaki (SM'85) received the B.S. degree (with honors) from Ain Shams University, Cairo, Egypt, in 1962, and the M.S. and Ph.D. degrees from the University of California, Berkeley, in 1966 and 1969, respectively, all in electrical engineering.

From 1962 to 1964, she was a Lecturer in the Department of Electrical Engineering, Ain Shams University. From 1965 to 1969, she held the position of Research Assistant in the Electronics Research Laboratory, University of California, Berkeley. She joined the Electrical Engineering Department, University of Maryland, College Park, MD, in 1970, where she is presently an Associate Professor. Her research interests are in the areas of electromagnetics, microwave circuits, optimization, computer-aided design, and numerical techniques.

Dr. Zaki is a member of Tau Beta Pi.